Biochimica et Biophysica Acta 1777 (2008) 711–718

Contents lists available at ScienceDirect

Biochimica et Biophysica Acta

journal homepage: www.elsevier.com/locate/bbabio

# Three-dimensional structure of respiratory complex I from *Escherichia coli* in ice in the presence of nucleotides

David J. Morgan, Leonid A. Sazanov *

*Medical Research Council, Dunn Human Nutrition Unit, Wellcome Trust/MRC Building, Hills Road, Cambridge CB2 2XY, UK*

ARTICLE INFO

*Article history:*
Received 23 January 2008
Received in revised form 7 March 2008
Accepted 25 March 2008
Available online 3 April 2008

*Keywords:*
Complex I
NADH:ubiquinone oxidoreductase
Membrane protein structure
Single particle analysis
Electron microscopy

ABSTRACT

Complex I (NADH:ubiquinone oxidoreductase) is the largest protein complex of bacterial and mitochondrial respiratory chains. The first three-dimensional structure of bacterial complex I in vitrified ice was determined by electron cryo-microscopy and single particle analysis. The structure of the *Escherichia coli* enzyme incubated with either $NAD^+$ (as a reference) or NADH was calculated to 35 and 39 Å resolution, respectively. The X-ray structure of the peripheral arm of *Thermus thermophilus* complex I was docked into the reference EM structure. The model obtained indicates that Fe–S cluster N2 is close to the membrane domain interface, allowing for effective electron transfer to membrane-embedded quinone. At the current resolution, the structures in the presence of $NAD^+$ or NADH are similar. Additionally, side-view class averages were calculated for the negatively stained bovine enzyme. The structures of bovine complex I in the presence of either $NAD^+$ or NADH also appeared to be similar. These observations indicate that conformational changes upon reduction with NADH, suggested to occur by a range of studies, are smaller than had been thought previously. The model of the entire bacterial complex I could be built from the crystal structures of subcomplexes using the EM envelope described here.

© 2008 Elsevier B.V. All rights reserved.

## 1. Introduction

Complex I (NADH:ubiquinone oxidoreductase, EC 1.6.5.3) is the first enzyme of the mitochondrial and bacterial respiratory chains. It catalyses the transfer of two electrons from NADH to quinone, coupled to the translocation of about 4 protons across the membrane, generating proton-motive force required for the synthesis of ATP [1,2]. The mitochondrial enzyme consists of 45 different subunits [3,4] and is one of the largest known membrane protein complexes, with a combined molecular mass of about 980 kDa. The prokaryotic enzyme (also referred to as NDH-1) is simpler and consists of 13–15 subunits with total mass of about 550 kDa [2,5]. Analogues of all conserved subunits of bacterial complex I are found in the mitochondrial enzyme [1], and they contain equivalent redox components [2]. Both the mitochondrial and bacterial enzymes have a characteristic L-shaped structure, with the hydrophobic arm embedded in the membrane and the hydrophilic peripheral arm protruding into the mitochondrial matrix or the bacterial cytoplasm [6–9]. Thus, the bacterial enzyme represents a 'minimal' model of complex I. Because of its central role in respiration, mutations in subunits of complex I can lead to many human neurodegenerative diseases [10]. Also, complex I has been suggested to be a major source of reactive oxygen species (ROS) in mitochondria, which can damage mtDNA and may be one of the causes of aging [11]. Parkinson's disease, at least in its sporadic form, may be caused by increased ROS production from malfunctioning complex I [12]. In contrast to most other membrane protein complexes of the respiratory chain, the atomic structure of the entire complex I is not yet known [13,14].

All structural models of intact complex I were obtained by electron microscopy, and the first was derived from negatively stained two-dimensional (2D) crystals of the *Neurospora crassa* enzyme [15,16]. Low-resolution structures of *Escherichia coli* [8], *N. crassa* [8,17], *Yarrowia lipolytica* [18] and *Aquifex aeolicus* [7] complex I have been obtained by single particle analysis of negatively stained samples. For the bovine enzyme, a 3D structure at 22 Å resolution was determined from frozen-hydrated samples [6].

The hydrophilic domain (peripheral arm) of complex I contains the NADH binding site and all known redox centres: the primary electron acceptor flavin mononucleotide (FMN) and 8 to 9 iron-sulphur (Fe–S) clusters [2,19,20]. Therefore, all electron transfer events before quinone reduction are likely to happen in the peripheral domain. Recently, we have determined the crystal structure of the hydrophilic domain of complex I from *Thermus thermophilus*, establishing the electron transfer pathway from the FMN, located near the tip of the peripheral arm, to the quinone binding site at the interface with the membrane arm [21]. The membrane spanning part of the enzyme seemingly lacks prosthetic groups, but it must contain essential

*Abbreviations:* CTF, contrast transfer function; DDM, dodecyl-maltoside; EEDQ, *N*-ethoxycarbonyl-2-ethoxy-1,2-dihydroquinoline; EM, electron microscopy; FEG, field emission gun; FMN, flavin mononucleotide; HEPES, 4-(2-hydroxyethyl)-1-piperazineethanesulfonic acid; MES, 2-(*N*-morpholino)-ethanesulfonic acid; ROS, reactive oxygen species

* Corresponding author. Fax: +44 1223 252915.
*E-mail address:* sazanov@mrc-dunn.cam.ac.uk (L.A. Sazanov).

0005-2728/$ – see front matter © 2008 Elsevier B.V. All rights reserved.
doi:10.1016/j.bbabio.2008.03.023

components of the proton translocating machinery. Sequence comparisons have suggested that the largest hydrophobic subunits of complex I, NuoL, NuoM and NuoN, are homologous to each other and that they have evolved from a common ancestor related to the $K^+$ or $Na^+/H^+$ antiporter family (Mrp) [22–25]. Therefore, these subunits are likely to participate in proton translocation. We have shown that two of these subunits, NuoL and NuoM, are at the distal end of the membrane domain, separated from the electron transfer pathway in the peripheral arm [26–28]. Recently, we determined the projection structure of the membrane domain of *E. coli* complex I at 8 Å resolution, showing the arrangement of about 60 transmembrane (TM) helices [48].

Although electron transfer events in the peripheral arm are now relatively well understood [14], the mechanism of coupling between electron transfer and proton pumping remains unknown. Two different models are being discussed: direct (redox-driven, for example employing modifications of the Q cycle or another chemical intermediate) [29] and indirect or conformation-driven coupling [2,22,28,30,31]. In support of the second model, significant conformational changes upon NAD(P)H or inhibitor (rotenone) binding to complex I have been suggested by cross-linking, proteolysis and kinetic studies with bovine and *E. coli* enzymes [32–36]. We have observed by electron microscopy that negatively stained *E. coli* complex I appears to have a more "open" conformation in the presence of NADH as compared to $NAD^+$ [36].

Crystallisation of the intact complex I, a very large and possibly flexible membrane protein assembly, remains a challenging task. Low-resolution models obtained by electron microscopy could provide a framework for building an atomic model of the entire complex from crystal structures of smaller subcomplexes. Complex I from *T. thermophilus* fragments during purification, which results in a preparation of peripheral domain only [5]. Therefore we have used preparations of *E. coli* enzyme as a general model of the intact bacterial enzyme. Because of the high degree of sequence conservation [2,37], the structures of bacterial enzymes from different sources are expected to be similar at low resolution. All previous single particle studies on bacterial complex I have been performed in negative stain. This technique provides high contrast images, but is subject to many potential artefacts, limiting the resolution and reliability of the resulting structures. The aim of this study was to perform the reconstruction using frozen-hydrated samples. The protein was kept in a buffered aqueous solution until it was flash-frozen, and so it should retain a native conformation. Furthermore, particles were imaged in ice over holes in the carbon support, avoiding any artefacts arising from interaction of the complex with carbon. Thus, the model obtained was expected to be sufficiently reliable to allow docking of crystal structures of subcomplexes. In view of the previously suggested conformational changes, two structures were obtained, in the presence of either $NAD^+$ or NADH.

## 2. Materials and methods

### 2.1. Materials

Chemicals were purchased from Sigma-Aldrich Company Ltd. (Dorset, England, UK) and Fluka Chemicals (Gillingham, UK). Dodecyl-β-D-maltoside was purchased from GLYCON GmbH (Luckenwalde, Germany). Complete™ protease inhibitor tablets were obtained from Roche Applied Science (Lewes, UK), Bio-scale DEAE column from Bio-Rad (Hemel Hempstead, UK), and other chromatography columns from Amersham Biosciences (St. Albans, UK). Electron microscopy stains and grids were purchased from Agar Scientific (Stansted, U.K).

### 2.2. Sample preparation

Complex I was purified from *E. coli* BL21 cells grown under limited oxygen conditions. Protein was purified by anion exchange and gel-filtration chromatography as described previously [9]. Complex I was stored under $LN_2$ in small aliquots in 20 mM Bis–Tris pH 6.0, 50 mM NaCl, 2 mM $CaCl_2$, 18% glycerol and ~2% DDM. The amount of detergent in protein stocks was high due to concentration at the end of purification. To reduce detergent and glycerol concentration, 50 μL of protein stock at 6.7 mg/mL was diluted 1:1 in buffer containing 0.15 M MES (pH 6.0), 0.15 M NaCl, 5 mM $CaCl_2$ and 0.03% DDM. Then an ice cold solution of 30% PEG 1000 in 20 mM MES (pH 6.0) was added to the diluted protein to a final concentration of 15%. The suspension was mixed by pipetting and incubated on ice for 15 min. Precipitated protein was pelleted at 4 °C by microfuge centrifugation at 12000 rpm for 10 min. The pellet was re-suspended in cryo buffer (20 mM MES (pH 6.0), 0.2 M NaCl, 2 mM $CaCl_2$ and 0.1% DDM) by vortexing for 2 h at 4 °C. Tests have shown that precipitated and re-suspended enzyme is fully functional: the levels of NADH:decylubiquinone activity and sensitivity to piericidin A are similar to that of freshly isolated complex I. The protein had a final concentration of approximately 5.7 mg/mL, and was stored on ice.

Complex I was incubated in either 3 mM $NAD^+$ or 3 mM NADH, and cryo buffer for 15 min at 4 °C, to achieve a final concentration of 3.4 mg/mL. This was performed immediately before grid preparation.

Bovine complex I was prepared either as described previously [31] or by a modified procedure involving addition of lipids [38]. The latter material was kindly provided by Dr. H. Pershad (MRC, Dunn Human Nutrition Unit) and was used for the final reconstructions shown here. Protein stock was diluted to ~15 μg/mL in 20 mM HEPES pH 7.0, 0.1 M NaCl, 10 mM $CaCl_2$, 0.03% DDM and 2 mM of either $NAD^+$ or NADH. Incubation in this mixture prior to negative staining was for ~5 min at 22 °C.

### 2.3. Specimen preparation for electron microscopy

Quantifoil micromachined holey carbon grids (300-mesh, R 1.2/1.3) (Agar Scientific, Stansted, U.K.) were glow discharged in air for 2 min to make them hydrophilic. Within 5 min after glow discharging, 4 μL of protein solution was applied to the grid. A thin film of protein solution was vitrified by blotting and rapid freezing using an FEI Vitrobot (FEI, Eindhoven, The Netherlands). Sample vitrification was performed according to the manufacturer's instructions, using a single blot of 2 s and a drain time of 5 s before rapid plunging into liquid ethane. Specimens were stored under liquid nitrogen.

For negative staining of bovine complex I particles, 400-mesh carbon coated copper grids (Agar Scientific, Stansted, U.K.) were glow discharged for 1 min and 5 μL of diluted protein was applied for 3 min. Sample was removed by blotting at the edge of the grid with Whatman filter paper (Kent, UK). The grid was washed twice using dilution buffer, blotted, and stained with freshly prepared 1% uranyl acetate solution for 10 s. Uranyl acetate was removed by blotting in order to achieve a relatively thick layer of stain with an air-drying time of about 2 min.

### 2.4. Cryo electron microscopy and image processing of E. coli complex I specimens

A Tecnai F20 transmission electron microscope (FEI, Eindhoven, The Netherlands, installed in MRC LMB) equipped with field emission gun (FEG) was used to image complex I from *E. coli* on Quantifoil grids. The microscope was operated in low-dose mode at a potential of 200 kV, providing an electron dose of approximately 10 e−/Å$^2$. Images were collected over a defocus range of 2.5–4.5 μm, at a calibrated magnification of 47700×. Images were recorded on Kodak SO-163 film (Agar Scientific, Stansted, U.K.) and developed in D-19 developer solution for 12 min.

Selected micrographs were digitised at a step size of 7 μm with a Zeiss SCAI scanner (Carl Zeiss Ltd., Oberkochen, Germany). Images were converted to MRC format and averaged over 2×2 pixels to give an effective pixel size of 14×14 μm, corresponding to 2.94 Å at the specimen. For each micrograph an average defocus value was calculated using the program CTFFIND2, particles were boxed and exported as stacks using Ximdisp from the MRC software suite [39,40]. Selected particles were separated from neighbouring particles and contained no other fragments. From 68 micrographs of complex I incubated in $NAD^+$, 6848 particles were picked and from 43 micrographs of complex I incubated in NADH, 4053 particles.

Particle stacks were converted to IMAGIC format and all subsequent processing was carried out using the IMAGIC-5 software suite [41].The CTF parameters of each micrograph were used to correct corresponding stacks of particles by phase flipping. The 6848 particle images of complex I incubated in $NAD^+$ were normalised and initially bandpass filtered to limit frequencies to a resolution range of 40–400 Å. A rotationally averaged total sum image was used as the reference for alignment and centring of the particles (5 iterations). Further multireference alignments were performed using loosely masked and centred class averages until images ceased to improve.

The data was then grouped into 100 class averages containing like views and the worst 30–40% rejected. Angular reconstitution was used to calculate the relative orientation between class averages for an *ab initio* model. Five rounds of iterative refinement were carried out, at each stage using forward projection to generate reference images of the model at angular intervals ranging from 24° to 13°. At each stage Euler angles assigned to 2D class averages were manually checked against reprojections of the 3D reconstruction, and if not in agreement the classes were discarded. During refinement, data filtering was reduced to incorporate a greater range to frequencies extending to 15 Å. Surface representations were calculated to correspond to a protein mass of 550 kDa, based on a protein density of 0.844 Da/Å$^3$. This level of contouring was also consistent with the expected overall dimensions of the molecule.

Reference images for the final model of complex I incubated in $NAD^+$ were used during the initial alignment of particles for complex I incubated in NADH. Further refinement was carried out as described above.

### 2.5. Electron microscopy and image processing of bovine complex I specimens

Negatively stained specimens of bovine complex I were viewed on a Tecnai 12 transmission electron microscope (FEI, Eindhoven, The Netherlands) equipped with a tungsten filament. The microscope was operated in low-dose mode at a potential of

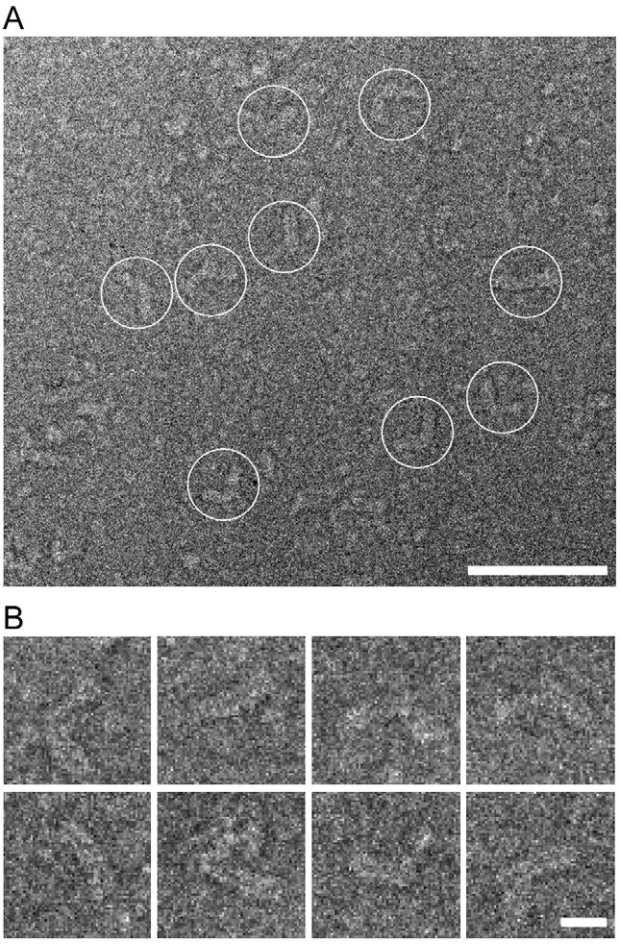


**Fig. 1.** A: Electron micrograph of *E. coli* complex I particles in vitreous ice (incubated in $NAD^+$; scale bar represents 50 nm). B: A gallery of single particles enlarged from 128×128 pixel images, uncorrected for contrast transfer function and prior to image processing (scale bar represents 10 nm).

100 kV. Images were collected at a magnification of 30 000× on Kodak SO-163 film, and developed as described above.

Micrographs were scanned at a step size of 7 μm and averaged over 2×2 pixels to give an effective pixel size of 14×14 μm, 4.67 Å per pixel at the specimen. Particles were picked from 9 micrographs of bovine complex I incubated in $NAD^+$ and 10 micrographs of the enzyme in NADH, generating 1188 and 1946 particles respectively. Particles were converted into IMAGIC format and processed using the IMAGIC-5 software suite. The contrast transfer function was not corrected since the resolution of negatively stained class averages was not expected to extend beyond the first zero. Centred particles were grouped into 24 classes, the best class averages were centred and masked for use as references in the next alignment. Refinement continued until class averages ceased to improve.

## 3. Results

### *3.1. Electron microscopy and image processing of E. coli complex I incubated in $NAD^+$*

Our previous cross-linking studies suggested that the conformations of the enzyme as purified (oxidised) and in the presence of $NAD^+$ are likely to be similar, whereas the addition of NADH (reduction of the enzyme) may induce conformational change [36]. In contrast to NADH, $NAD^+$ has a very low affinity towards the oxidised enzyme (~1 mM) [14], and so may not be bound to it, or only weakly interact with it, under our experimental conditions (3 mM $NAD^+$). Furthermore, a range of gel-filtration chromatography experiments suggested that in the presence of $NAD^+$, the complex is similar to, or slightly more stable than, the control. However, it is destabilised (fragmented) in the presence of NADH under less favourable conditions (high temperature, prolonged incubation, high/low pH; data not shown). To facilitate the comparison of structures in the presence of nucleotides, the reference structure was determined in $NAD^+$, even though it may not be bound to the protein. Purified and hydrated complex I was analysed on copper EM grids by electron cryo-microscopy. When the thin layer of vitrified ice with embedded protein was imaged through 1.2 μm holes in the carbon support film, individual particles were clearly visible (Fig. 1A). The outline of individual particles is consistent with the "L" shaped structure seen in negatively stained images of complex I from a variety of organisms [6,8,16,18]. Protein on a continuous support film is constrained by interactions with the flat carbon into preferred orientations. Therefore, negatively stained complex I is seen only from the side in either a "flip" or "flop" orientation [36]. Complex I in vitreous ice is free to adopt effectively any orientation providing a greater variety of views, as evident in the unprocessed particle images (Fig. 1B).

Five iterations of multivariate statistical analysis, classification, angular reconstitution and three-dimensional reconstruction [42,43]

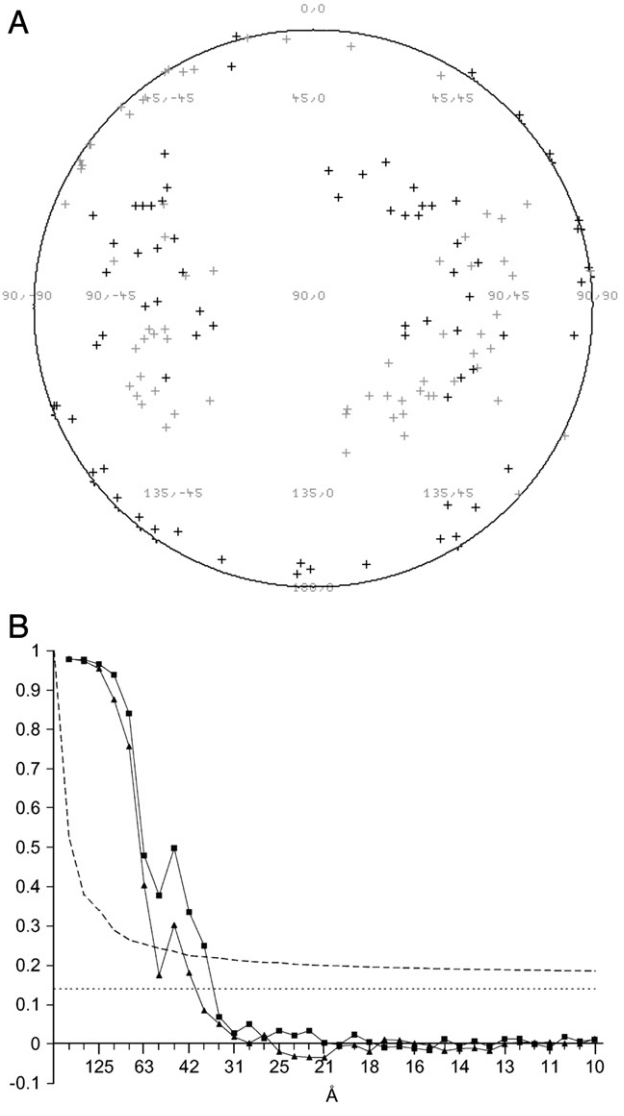


**Fig. 2.** A: Distribution of Euler angles for the 146 class average images of *E. coli* complex I incubated in $NAD^+$. Coordinates describe beta and gamma Euler angles. Black crosses show class averages assigned gamma angles in the hemisphere −90, 0, −90, and grey crosses in the hemisphere 90, 180, −90. B: Fourier shell correlation curves for three-dimensional reconstructions of complex I in $NAD^+$ (squares) and NADH (triangles). A threshold of three times noise correlation is shown as a dashed line and at FSC=0.14 (used to estimate resolution here [44]) as a dotted line.

were used in the building of an *ab initio* model, and its refinement. Forward projections into the asymmetric triangle were used as references for each new round. At the final stage of refinement, 255 class averages were generated after aligning the 6848 particles to 13° separated reference images. Euler angles between class averages were calculated by angular reconstitution, the worst class averages were removed and the remainder was checked for correct orientation, resulting in 146 views (containing 3897 particles). The distribution of the Euler angles (Fig. 2A) shows an over representation of the protein in the "flip" and "flop" orientations around the 90°, 45° and 90°, −45° positions. The freedom to adopt any orientation may have been limited by ice thickness. The length of the membrane arm (*ca.* 200 Å), or the *ca.* 350 Å distance between distal points on the two arms could begin to approach the thickness of ice. Alternatively, side views may be over represented because they are identified more readily in micrographs than end-on views. To check for bias, an attempt to reduce the relative number of side-view particles during refinement was made by increasing a proportion of rejected worst particles in corresponding classes. This did not result in any noticeable changes in the model, and so was not implemented in the final refinements. The Fourier shell correlation between two half sets of class averages was used to determine the overall resolution of the final model. At a correlation of 0.14 [44] the resolution is 35 Å (Fig. 2B), and all maps were filtered to a corresponding high frequency cut-off value for display here.

### 3.2. Electron microscopy and image processing of E. coli complex I incubated in NADH

The protein was incubated with NADH for about 15 min at pH 6.0. These conditions do not result in the destabilisation of the complex, as determined by gel-filtration chromatography (data not shown). The raw images were acquired in a similar manner to those used for $NAD^+$ reconstruction. The final model of complex I incubated in $NAD^+$ was forward projected to generate a set of 2D references. This set was used for an initial alignment of the 4053 particles of complex I incubated in NADH. Then the model was refined as described above. The final reconstruction is comprised of 103 class averages (containing 1730 particles). The Fourier shell correlation was calculated between two half sets of class averages; at a value of 0.14 the resolution is 39 Å (Fig. 2B).

### 3.3. Three-dimensional reconstruction of E. coli complex I

Despite the asymmetrical shape of complex I, the similarity in size of the two arms sometimes resulted in incorrect Euler angle assignment by the software. Therefore, it was necessary at each stage to check manually for correct peripheral and membrane arm orientation, since by eye it was still possible to distinguish the features of each arm. Two-dimensional reprojections of the 3D density map and class averages viewed along the same Euler angles are shown in Fig. 3. Comparison of

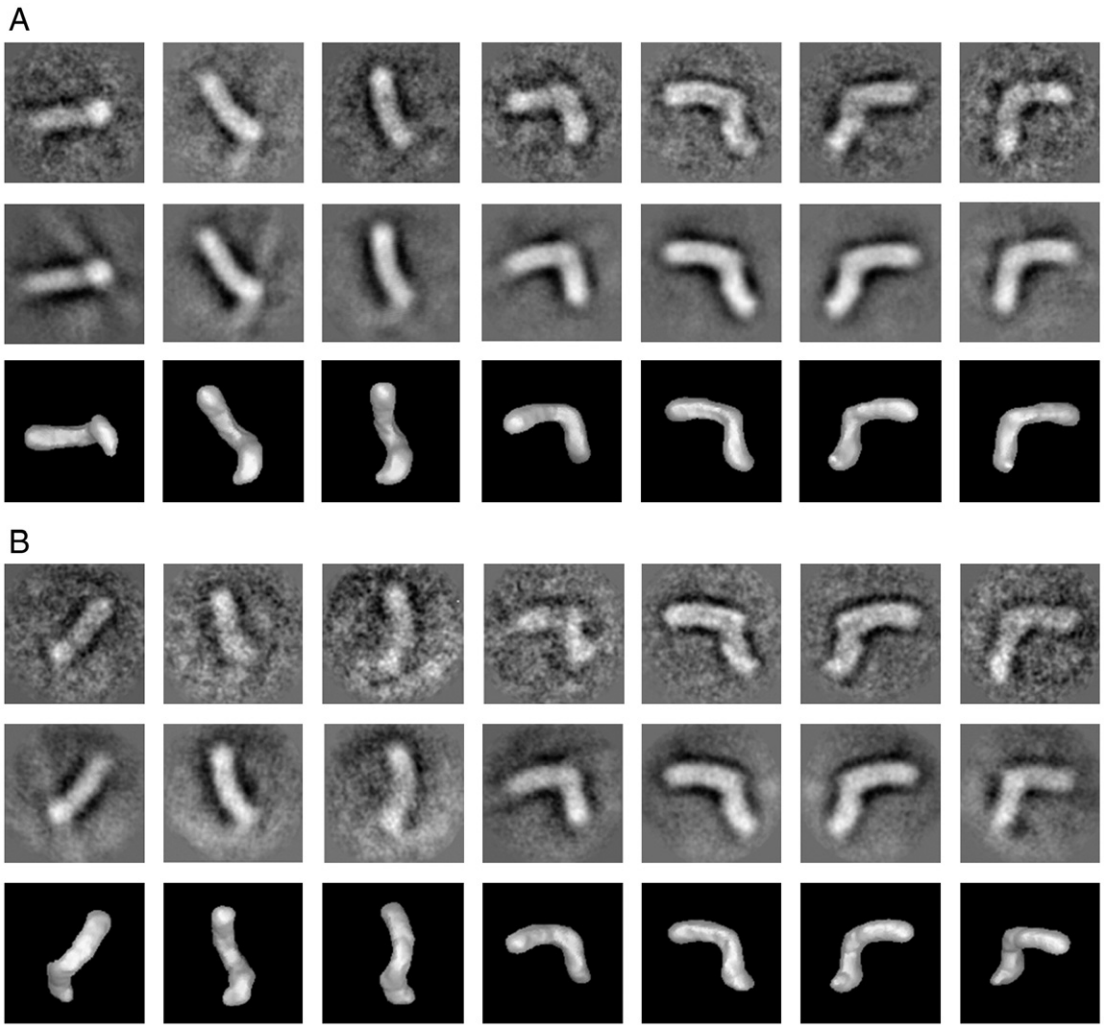


**Fig. 3.** Galleries of single particle processing steps for $NAD^+$ (A) and NADH (B) data. A selection of characteristic class averages is shown in the top row. Using the same Euler angles, the corresponding 2D reprojections of the 3D reconstruction are shown in the second row, and a surface render of the 3D reconstruction in row 3.

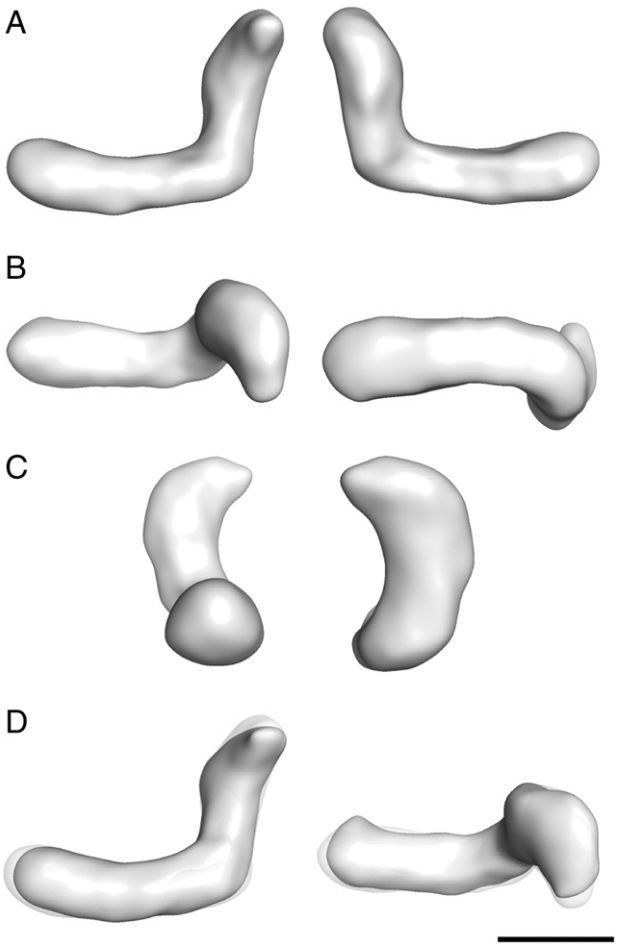


**Fig. 4.** Surface rendered views of the 3D reconstruction of *E. coli* complex I. The complex incubated in $NAD^+$ is shown in the "flip" and "flop" orientations, rotated 180° to each other about the axis of the peripheral arm (A); viewed from each end of the peripheral arm axis (B) and membrane arm axis (C). D: The models of complex I incubated in $NAD^+$ (transparency) and NADH (solid) are overlaid. The scale bar represents 10 nm.

the reprojections and class averages clearly shows discernable differences between the two arms, and confirms that they are represented correctly in the reconstruction. Consistently, side-view averages resemble reconstructions of similar views from negative stain [36], allowing us to recognise the characteristic features of each arm and thus assign them in the reconstruction (Fig. 4). Apparent variations in the relative lengths of the arms in class averages are due to different orientations of the molecule relative to the observer, as can be seen from comparison with the reprojections. The structural differences between arms are also present in the corresponding surface representations of the complex I models (bottom rows in Fig. 3), confirming correct angular reconstitution.

Viewed from the side in flip and flop orientations (Fig. 4A), the model of *E. coli* complex I reveals the characteristic L-shape as reported previously [9,36], with the peripheral arm positioned vertically and the membrane arm horizontal. The membrane arm is about 200 Å long and 40 Å thick, consistent with an average lipid bilayer thickness, whereas the peripheral arm would extend about 130–140 Å above the bilayer. Viewed from above and below in Fig. 4B the membrane arm has a slight curvature consistent with models published for *Y. lipolytica* complex I [18]. The peripheral arm increases in width as it extends above the membrane arm, reaching ~100 Å at the widest point. This feature has not been observed previously in class averages or 3D models reconstructed from negatively stained particles of *E. coli* complex I [8], and is consistent with the characteristic Y-shape of the peripheral arm seen in its crystal structure [20,21].

The structure of the hydrophilic domain of *T. thermophilus* complex I has been solved at high resolution [21], and provides features that allow its positioning within this low-resolution model of the intact bacterial enzyme. Subunits Nqo4 and Nqo6 in the lower part of the X-ray structure (as shown in Fig. 5) form an interface with the membrane domain. Manual docking of the X-ray structure into the reconstruction of *E. coli* complex I as shown in Fig. 5, consistent with our assignment of the peripheral arm, leaves a minimal proportion of the X-ray structure outside the EM density. Two lobes at the top of the crystal structure, formed mostly by subunits Nqo1 and Nqo3, fit well into the density. In an alternative theoretically possible fit, rotated by about 180° along vertical, the Nqo1 lobe would protrude out of the density. Additional confirmation of the fit shown in Fig. 5 is provided by α helix H1, which protrudes about 25 Å from subunit Nqo6 [21]. This helix has a polar upper surface and hydrophobic lower surface. It is likely to extend into the surface of the membrane domain, consistent with the orientation shown in Fig. 5. In an alternative fit (rotated by 180°) this helix would protrude on its own far out from the EM density. In the best fit as shown here, a few surface regions of the crystal structure still extend beyond EM density; this is most likely due to the limited resolution of the reconstruction.

To assess whether any conformational changes due to substrate binding and enzyme reduction can be observed, data were collected

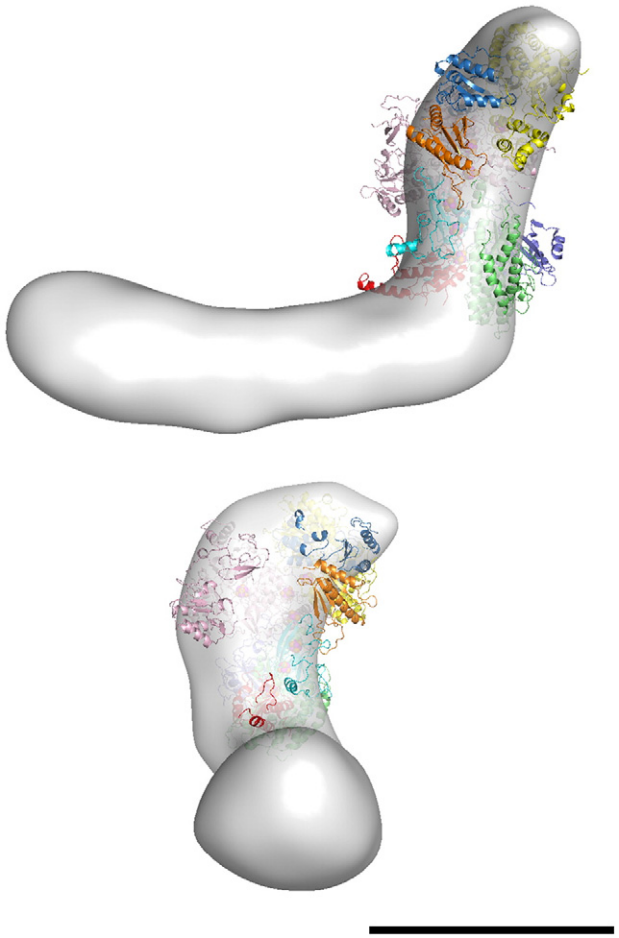

**Fig. 5.** Modelling the structure of complex I. Manual docking of the *T. thermophilus* peripheral arm structure (PDB code 2FUG) [21] into the model of *E. coli* complex I incubated in $NAD^+$. Subunits are coloured as in [21]: Nqo1 — yellow, Nqo2 — blue, Nqo3 — salmon, Nqo4 — green, Nqo5 — violet, Nqo6 — red, Nqo9 — marine, and Nqo15 — brown. Metal sites are shown as red spheres for Fe atoms and yellow spheres for S atoms. "Side" (flip) and "front" (rotated 90° about the axis of the peripheral arm) views are shown. The scale bar represents 10 nm.

for *E. coli* complex I incubated in the presence of NADH, while all other conditions were kept identical to the $NAD^+$ reconstruction. The model of complex I in NADH (Fig. 4D) shows no significant differences to the structure in $NAD^+$, at the current resolution. Only at the extremities of the membrane and peripheral arm do the models differ slightly when they are superimposed (Fig. 4D). Without higher resolution data, it is not possible to discern whether these differences are due to under-representation in the data, or to small structural changes.

### 3.4. Electron microscopy and image processing of bovine complex I incubated in $NAD^+$ and NADH

Previously, significant changes in cross-linking and proteolysis patterns in the presence of NADH were reported for the bovine enzyme [33,34,45]. Therefore, we decided to examine whether any conformational change could be observed by EM in bovine complex I. Previous studies were performed with the enzyme purified by a series of precipitation steps in bile salts and which was likely to contain many bound native lipids [46]. The protein used in our studies was purified by chromatography in dodecyl-maltoside (DDM) [31,38] and may have different properties. Therefore, we verified the cross-linking results using the same samples as used for EM here. In the presence of zero-length cross-linker EEDQ, addition of NADH to bovine complex I resulted in a reduction in the number of cross-links involving the 49 and 75 kDa subunits, as compared to $NAD^+$ or control (J. Berrisford and L. Sazanov, unpublished data), in agreement with previous observations [33,45]. Electron micrographs of the negatively stained particles reveal uniform L-shaped monomers (Fig. 6A). Although almost twice the size of the *E. coli* complex I, the bovine enzyme exhibits the same L-shape in single particle images and reconstructions [6]. Single particles of bovine complex I, incubated in the two nucleotides, were picked and processed separately and independently, without any references. Class averages stabilised during refinement. Reducing the number of classes from 24 to 6 produced similar looking averages in both the flip and flop orientation. $NAD^+$ and NADH data sets both showed the enzyme with a ~3:1 ratio of flip/flop views, four of which are shown in Fig. 6A. The resolution of the averages is difficult to estimate reliably because of the relatively small number of particles in each class, but is not expected to be better than about 30–35 Å.

As was observed in our cryo-EM 3D reconstructions of *E. coli* complex I, at the current resolution there is no significant difference in size or shape between the enzyme incubated in $NAD^+$ or NADH.

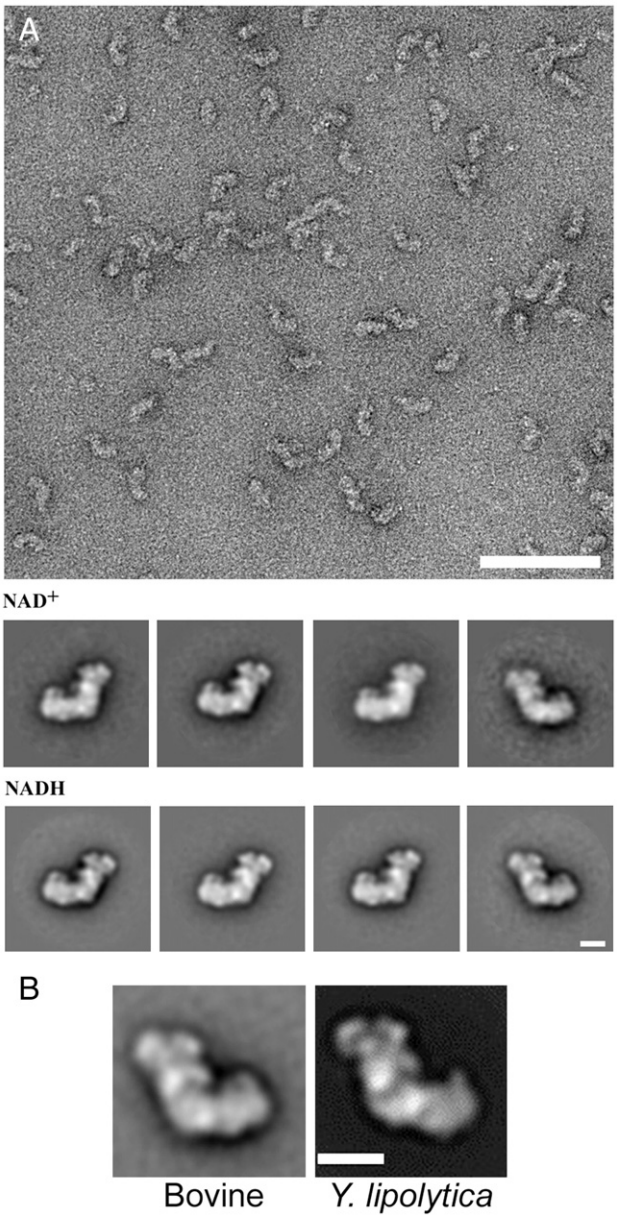


**Fig. 6.** EM of bovine enzyme. A: Electron micrograph of bovine complex I in negative stain (scale bar represents 100 nm). Below are shown the characteristic class averages of the complex incubated in $NAD^+$ and NADH. Protein interaction with the carbon layer leads to the preferred "flip" and "flop" orientations seen in the electron micrograph and averaged images (scale bar represents 10 nm). B: Comparison of side views of bovine (this work) and *Y. lipolytica* (reproduced with permission from Fig. 3 in Ref. [18]) complex I.

## 4. Discussion

We have determined the first cryo-EM 3D structure of the intact bacterial complex I. The protein was frozen-hydrated in ice and particles were imaged in areas without carbon support. Such a reconstruction should be free from artefacts of the negative staining technique, which include effects of high final metal salt concentration, unfavourable pH of some stains, protein flattening on the carbon support during the drying process and other limitations to the resolution. Overall, our structure shows some similarity to the previous 3D reconstruction of negatively stained *E. coli* enzyme [8]. However, it can be seen (in comparison with Fig. 4 in Ref. [8]) that although side views agree reasonably well, with similar features and dimensions of the two arms, the structure in negative stain was severely flattened in the 3rd dimension, presumably due to protein drying on the carbon support. These effects were especially pronounced in the peripheral arm and made its structure incompatible with the Y-shape of the crystal structure. This is in contrast to our model, which allows clear fit of the crystal structure into the density (Figs. 4 and 5). Flattening effects can be minimised with a "deep stain" technique, used for the 3D reconstruction of mitochondrial complex I from *Y. lipolytica* [18]. In that case, both the Y-shape of the peripheral arm and the curvature of the membrane domain were preserved and agree well with our model, even though the mitochondrial enzyme contains about 30 additional, mostly small, subunits.

The resolution of our reconstructions is lower than what we expected from the raw images, which were acquired on a FEG microscope. CTF rings in Fourier transforms are visible to beyond 12 Å resolution (not shown), indicating that data extend at least to that resolution. Our attempts to refine the model further and improve the resolution by using FREALIGN software [47] were not successful (data not shown). The most likely reason for the low resolution in these reconstructions is an inherent flexibility of complex I, particularly variations in the angle between the two arms, as observed previously for the *E. coli* enzyme [8]. During averaging and reconstruction this would result in "blurring" of the structure, as we have seen previously for side views [36]. In the reconstruction from negatively stained samples of *Y. lipolytica* complex I by the random conical tilt technique, such flexibility resulted in several somewhat different structures [18].

However, for frozen-hydrated specimens the classification into subpopulations of particles does not seem feasible due to the low contrast and signal-to-noise ratio in individual raw images. One possibility to improve the resolution of the 3D reconstructions in ice could be to use intact thermophilic complex I, which shows much less "blurring" in side views [7], presumably because it is more stable.

Electron transfer in the peripheral arm proceeds from NADH to FMN, bound to the Nqo1 subunit near the tip of the arm, and then through a chain of six conserved Fe–S clusters to the terminal high-potential cluster N2, which is likely to donate electrons to the quinone [14]. Cluster N2 is coordinated within subunit Nqo6 at the interface with subunit Nqo4 [21]. In the model shown in Fig. 5, these subunits are in contact with the membrane domain. In this arrangement, cluster N2 will be within 10 Å or so from the membrane domain surface. This will allow the quinone head group to be sufficiently close to N2 for effective electron transfer, while the hydrophobic tail of quinone can remain within the membrane environment. A likely channel for quinone access in this area of the membrane arm was identified in our projection map of the membrane domain of *E. coli* complex I [48]. In contrast, the best fit of the crystal structure into the EM map as proposed for *Y. lipolytica* enzyme would place cluster N2 about 60 Å from the membrane domain [49]. This position seems to be unlikely, as the hydrophobic ubiquinone would have to be somehow re-positioned close to N2 for electron transfer to occur. On the other hand, alternative fits (3 and 4 in Fig. 5 in Ref. [49]) agree reasonably well with our model in the overall orientation, even though cluster N2 in these fits is still 52 or 40 Å from the membrane domain. At least some of this discrepancy could be attributed to the additional protein mass in the mitochondrial enzyme.

The mechanism by which electron transfer in complex I is coupled to proton translocation remains unsolved. Cross-linking, limited proteolysis and kinetic studies clearly indicate, both for the bacterial [36] and mitochondrial [33–35,45] enzymes, that reduction by NADH induces significant conformational changes. Therefore, it is discussed widely that the coupling mechanism may involve long-range conformational changes [14,22,31,50].We have observed previously from single particle analysis of negatively stained particles that *E. coli* complex I presents an "open" conformation in the presence of NADH, with increased apparent thickness to both arms of the enzyme [36]. This observation was consistent with a decreased number of inter-subunit cross-links in the presence of NADH. However, by cryo-EM (Figs. 3 and 4) we do not observe such a dramatic change and the $NAD^+$/NADH reconstructions look similar at the current resolution. It is possible that any differences have been averaged out due to the low resolution and possible flexibility in the structure. If any conformational changes do happen, they may be visible at higher resolution. This proposal would be consistent with cross-link patterns changing much more dramatically when zero-length cross-linker (EEDQ) is used rather than reagents with a linker of about 10 Å [36]. The reason for the large structural changes that were observed in negative stain is likely to be the destabilisation of the *E. coli* complex in the presence of NADH, mentioned above. It is particularly significant at pH values outside of the favourable range (5.5–6.5). The protein is exposed to negative stain only for a short time. However, in uranyl acetate the pH is likely to be about 4, which might be sufficient to destabilise complex I in the presence of NADH (but not in $NAD^+$). Such destabilisation could lead to an increased flattening effect on the carbon, and explain the apparent increased thickness of the complex in the presence of NADH [36].

We also examined whether any conformational change could be observed with bovine complex I. Unlike the negatively stained *E. coli* enzyme [36], in uranyl acetate bovine complex I has a similar conformation in the presence of either $NAD^+$ or NADH (Fig. 6). This possibly reflects the fact that the bovine enzyme is stable over a wider pH range and at higher salt concentrations [51] compared to the *E. coli* complex, and so it may not be significantly destabilised in the presence of NADH. Similar to our *E. coli* reconstructions in ice, any functional conformational changes may be discernable only at higher resolution. Both *E. coli* [9] and bovine [38] enzymes show high activity with quinone as acceptor only in the presence of lipids added to the assay buffer. In principle, it cannot be excluded that larger conformational changes may happen when enzyme is embedded into the lipid membrane, and if a proton gradient is present.

The overall shape of the bovine enzyme in side view is very similar between different class averages (Fig. 6), indicating a relative conformational stability of the complex and reliability of the observed distinctive features. The overall dimensions of the complex are similar between the bovine and *E. coli* enzymes. However, bovine complex I has generally "thicker" arms and some additional features, such as subdomains protruding at the distal end of the membrane arm and in the middle of peripheral arm, facing each other. These features must reflect the additional protein mass in the mitochondrial enzyme. Our averaged images very closely resemble side views of the *Y. lipolytica* enzyme [18] (Fig. 6B), and a previously published bovine side-view average (Fig. 5A in Ref. [52]). The fine features of both arms of the complex agree very well (Fig. 6B), indicating that the 3D structures of the bovine and *Y. lipolytica* enzymes are also likely to be very similar. The peripheral arm branches into two lobes in these organisms, creating the Y-shape observed in the *T. thermophilus* crystal structure. These features are absent from the cryo-EM reconstruction of the bovine enzyme at nominally higher resolution [6], suggesting that the *Y. lipolytica* 3D structure is currently a more reliable 3D model for the mammalian enzyme.

Our observations do not exclude conformational changes as part of a coupling mechanism, but indicate that they may be less dramatic than thought previously. Apart from cross-linking and kinetic evidence, the overall architecture of the complex strongly suggests a requirement for long-range communication within the enzyme. The two antiporter-like subunits NuoL and NuoM, likely to be involved in proton pumping, are a long way from the peripheral arm and the electron transfer pathway [26,48]. Therefore, some form of conformational coupling is needed, which would involve possibly not large-scale, as demonstrated here, but necessarily long-range conformational changes. A combination of conformational and direct coupling is also quite likely because of high proton/electron stoichiometry of complex I [14,22,27]. Atomic resolution structures of different states of the enzyme during the catalytic cycle will be needed in order to answer these mechanistic questions. Our EM model of the intact enzyme should be helpful in building up an atomic model of the entire complex from the structures of its subcomplexes, once they are determined.

## Acknowledgements

This work was supported by the Medical Research Council. We thank Dr. H. Pershad, Martin King and Dr. J. Hirst (The MRC Dunn Human Nutrition Unit) for samples of bovine complex I.

## References

[1] J.E. Walker, The NADH — ubiquinone oxidoreductase (complex I) of respiratory chains, Q. Rev. Biophys. 25 (1992) 253–324.
[2] T. Yagi, A. Matsuno-Yagi, The proton-translocating NADH-quinone oxidoreductase in the respiratory chain: the secret unlocked, Biochemistry 42 (2003) 2266–2274.
[3] J. Carroll, I.M. Fearnley, R.J. Shannon, J. Hirst, J.E. Walker, Analysis of the subunit composition of complex I from bovine heart mitochondria, Mol. Cell. Proteomics 2 (2003) 117–126.
[4] J. Carroll, I.M. Fearnley, J.M. Skehel, R.J. Shannon, J. Hirst, J.E. Walker, Bovine complex I is a complex of 45 different subunits, J. Biol. Chem. 281 (2006) 32724–32727.
[5] P. Hinchliffe, J. Carroll, L.A. Sazanov, Identification of a novel subunit of respiratory complex I from *Thermus thermophilus*, Biochemistry 45 (2006) 4413–4420.
[6] N. Grigorieff, Three-dimensional structure of bovine NADH:ubiquinone oxidoreductase (complex I) at 22 A in ice, J. Mol. Biol. 277 (1998) 1033–1046.
[7] G. Peng, G. Fritzsch, V. Zickermann, H. Schagger, R. Mentele, F. Lottspeich, M. Bostina, M. Radermacher, R. Huber, K.O. Stetter, H. Michel, Isolation, characterization and electron microscopic single particle analysis of the NADH:ubiquinone oxidoreductase (complex I) from the hyperthermophilic eubacterium *Aquifex aeolicus*, Biochemistry 42 (2003) 3032–3039.

[8] V. Guenebaut, A. Schlitt, H. Weiss, K. Leonard, T. Friedrich, Consistent structure between bacterial and mitochondrial NADH:ubiquinone oxidoreductase (complex I), J. Mol. Biol. 276 (1998) 105–112.
[9] L.A. Sazanov, J. Carroll, P. Holt, L. Toime, I.M. Fearnley, A role for native lipids in the stabilization and two-dimensional crystallization of the *Escherichia coli* NADH-ubiquinone oxidoreductase (Complex I), J. Biol. Chem. 278 (2003) 19483–19491.
[10] A.H. Schapira, Human complex I defects in neurodegenerative diseases, Biochim. Biophys. Acta 1364 (1998) 261–270.
[11] R.S. Balaban, S. Nemoto, T. Finkel, Mitochondria, oxidants, and aging, Cell 120 (2005) 483–495.
[12] T.M. Dawson, V.L. Dawson, Molecular pathways of neurodegeneration in Parkinson's disease, Science 302 (2003) 819–822.
[13] M. Saraste, Oxidative phosphorylation at the fin de siecle, Science 283 (1999) 1488–1493.
[14] L.A. Sazanov, Respiratory complex I: mechanistic and structural insights provided by the crystal structure of the hydrophilic domain, Biochemistry 46 (2007) 2275–2288.
[15] K. Leonard, H. Haiker, H. Weiss, Three-dimensional structure of NADH: ubiquinone reductase (complex I) from *Neurospora* mitochondria determined by electron microscopy of membrane crystals, J. Mol. Biol. 194 (1987) 277–286.
[16] G. Hofhaus, H. Weiss, K. Leonard, Electron microscopic analysis of the peripheral and membrane parts of mitochondrial NADH dehydrogenase (complex I), J. Mol. Biol. 221 (1991) 1027–1043.
[17] V. Guenebaut, R. Vincentelli, D. Mills, H. Weiss, K.R. Leonard, Three-dimensional structure of NADH-dehydrogenase from *Neurospora crassa* by electron microscopy and conical tilt reconstruction, J. Mol. Biol. 265 (1997) 409–418.
[18] M. Radermacher, T. Ruiz, T. Clason, S. Benjamin, U. Brandt, V. Zickermann, The three-dimensional structure of complex I from *Yarrowia lipolytica*: a highly dynamic enzyme, J. Struct. Biol. 154 (2006) 269–279.
[19] T. Ohnishi, Iron–sulfur clusters/semiquinones in complex I, Biochim. Biophys. Acta 1364 (1998) 186–206.
[20] P. Hinchliffe, L.A. Sazanov, Organization of iron–sulfur clusters in respiratory complex I, Science 309 (2005) 771–774.
[21] L.A. Sazanov, P. Hinchliffe, Structure of the hydrophilic domain of respiratory complex I from *Thermus thermophilus*, Science 311 (2006) 1430–1436.
[22] T. Friedrich, Complex I: a chimaera of a redox and conformation-driven proton pump? J. Bioenerg. Biomembr. 33 (2001) 169–177.
[23] I.M. Fearnley, J.E. Walker, Conservation of sequences of subunits of mitochondrial complex I and their relationships with other proteins, Biochim. Biophys. Acta 1140 (1992) 105–134.
[24] R. Kikuno, T. Miyata, Sequence homologies among mitochondrial DNA-coded URF2, URF4 and URF5, FEBS Lett. 189 (1985) 85–88.
[25] C. Mathiesen, C. Hagerhall, The 'antiporter module' of respiratory chain complex I includes the MrpC/NuoK subunit — a revision of the modular evolution scheme, FEBS Lett. 549 (2003) 7–13.
[26] E.A. Baranova, D.J. Morgan, L.A. Sazanov, Single particle analysis confirms distal location of subunits NuoL and NuoM in *Escherichia coli* complex I, J. Struct. Biol. 159 (2007) 238–242.
[27] L.A. Sazanov, J.E. Walker, Cryo-electron crystallography of two sub-complexes of bovine complex I reveals the relationship between the membrane and peripheral arms, J. Mol. Biol. 302 (2000) 455–464.
[28] P.J. Holt, D.J. Morgan, L.A. Sazanov, The location of NuoL and NuoM subunits in the membrane domain of the *Escherichia coli* complex I: implications for the mechanism of proton pumping, J. Biol. Chem. 278 (2003) 43114–43120.
[29] P.L. Dutton, C.C. Moser, V.D. Sled, F. Daldal, T. Ohnishi, A reductant-induced oxidation mechanism for complex I, Biochim. Biophys. Acta 1364 (1998) 245–257.
[30] U. Brandt, Energy converting NADH:quinone oxidoreductase (complex I), Annu. Rev. Biochem. 75 (2006) 69–92.
[31] L.A. Sazanov, S.Y. Peak-Chew, I.M. Fearnley, J.E. Walker, Resolution of the membrane domain of bovine complex I into subcomplexes: implications for the structural organization of the enzyme, Biochemistry 39 (2000) 7229–7235.
[32] J.A. Gondal, W.M. Anderson, The molecular morphology of bovine heart mitochondrial NADH-ubiquinone reductase. Native disulfide-linked subunits and rotenone-induced conformational changes, J. Biol. Chem. 260 (1985) 12690–12694.
[33] G. Belogrudov, Y. Hatefi, Catalytic sector of complex I (NADH:ubiquinone oxidoreductase): subunit stoichiometry and substrate-induced conformation changes, Biochemistry 33 (1994) 4571–4576.
[34] M. Yamaguchi, G.I. Belogrudov, Y. Hatefi, Mitochondrial NADH-ubiquinone oxidoreductase (complex I). Effect of substrates on the fragmentation of subunits by trypsin, J. Biol. Chem. 273 (1998) 8094–8098.
[35] N. Hano, Y. Nakashima, K. Shinzawa-Itoh, S. Yoshikawa, Effect of the side chain structure of coenzyme Q on the steady state kinetics of bovine heart NADH: coenzyme Q oxidoreductase, J. Bioenerg. Biomembr. 35 (2003) 257–265.
[36] A.A. Mamedova, P.J. Holt, J. Carroll, L.A. Sazanov, Substrate-induced conformational change in bacterial complex I, J. Biol. Chem. 279 (2004) 23830–23836.
[37] T. Yano, S.S. Chu, V.D. Sled, T. Ohnishi, T. Yagi, The proton-translocating NADH-quinone oxidoreductase (NDH-1) of thermophilic bacterium *Thermus thermophilus* HB-8. Complete DNA sequence of the gene cluster and thermostable properties of the expressed NQO2 subunit, J. Biol. Chem. 272 (1997) 4201–4211.
[38] M.S. Sharpley, R.J. Shannon, F. Draghi, J. Hirst, Interactions between phospholipids and NADH:ubiquinone oxidoreductase (complex I) from bovine mitochondria, Biochemistry 45 (2006) 241–248.
[39] J.M. Smith, Ximdisp — a visualization tool to aid structure determination from electron microscope images, J. Struct. Biol. 125 (1999) 223–228.
[40] R.A. Crowther, R. Henderson, J.M. Smith, MRC image processing programs, J. Struct. Biol. 116 (1996) 9–16.
[41] M. van Heel, G. Harauz, E.V. Orlova, R. Schmidt, M. Schatz, A new generation of the IMAGIC image processing system, J. Struct. Biol. 116 (1996) 17–24.
[42] M. van Heel, B. Gowen, R. Matadeen, E.V. Orlova, R. Finn, T. Pape, D. Cohen, H. Stark, R. Schmidt, M. Schatz, A. Patwardhan, Single-particle electron cryo-microscopy: towards atomic resolution, Q. Rev. Biophys. 33 (2000) 307–369.
[43] M. Van Heel, Angular reconstitution: a posteriori assignment of projection directions for 3D reconstruction, Ultramicroscopy 21 (1987) 111–123.
[44] P.B. Rosenthal, R. Henderson, Optimal determination of particle orientation, absolute hand, and contrast loss in single-particle electron cryomicroscopy, J. Mol. Biol. 333 (2003) 721–745.
[45] S.D. Patel, C.I. Ragan, Structural studies on mitochondrial NADH dehydrogenase using chemical cross-linking, Biochem. J. 256 (1988) 521–528.
[46] Y. Hatefi, Preparation and properties of NADH: ubiquinone oxidoreductase (complex I), EC 1.6.5.3, Methods Enzymol. 53 (1978) 11–14.
[47] N. Grigorieff, FREALIGN: high-resolution refinement of single particle structures, J. Struct. Biol. 157 (2007) 117–125.
[48] E.A. Baranova, P.J. Holt, L.A. Sazanov, Projection structure of the membrane domain of *Escherichia coli* respiratory complex I at 8 A resolution, J. Mol. Biol. 366 (2007) 140–154.
[49] T. Clason, V. Zickermann, T. Ruiz, U. Brandt, M. Radermacher, Direct localization of the 51 and 24 kDa subunits of mitochondrial complex I by three-dimensional difference imaging, J. Struct. Biol. 159 (2007) 433–442.
[50] U. Brandt, S. Kerscher, S. Drose, K. Zwicker, V. Zickermann, Proton pumping by NADH: ubiquinone oxidoreductase. A redox driven conformational change mechanism? FEBS Lett. 545 (2003) 9–17.
[51] N. Hano, Y. Nakashima, K. Shinzawa-Itoh, H. Terada, S. Yoshikawa, Effect of pH on the steady state kinetics of bovine heart NADH: coenzyme Q oxidoreductase, J. Bioenerg. Biomembr. 35 (2003) 419–425.
[52] E. Schafer, H. Seelert, N.H. Reifschneider, F. Krause, N.A. Dencher, J. Vonck, Architecture of active mammalian respiratory chain supercomplexes, J. Biol. Chem. 281 (2006) 15370–15375.